þÿ±-Synuclein Aggregation Inhibitory Prunolides a
þÿDibrominated ²-Carboline Sulfamate from the As
Synoicum prunum

Holland, Darren C

2022-02-25

Holland , D C , Prebble , D W , Er , S , Hayton , J B , Robertson , L P , Avery , V M ,
þÿDomanskyi , A , Kiefel , M J , Hooper , J N A & Carroll , A R 2022 , ' =
þÿInhibitory Prunolides and a Dibrominated ²-Carboline Sulfamate from t
prunum ' , Journal of Natural Products , vol. 85 , no. 2 , pp. 441-452 . https://doi.org/10.1021/acs.jnatprod.1c01172

http://hdl.handle.net/10138/353211
https://doi.org/10.1021/acs.jnatprod.1c01172

unspecified
acceptedVersion

α-Synuclein Aggregation Inhibitory Prunolides and a Dibrominated β-Carboline Sulfamate from the Ascidian *Synoicum prunum*

Darren C. Holland,[†,‡] Dale W. Prebble,[†,‡] Safak Er,[§,^] Joshua B. Hayton,[†,‡] Luke P. Robertson,[†,‡] Vicky M. Avery,[†,‡,∥] Andrii Domanskyi,[§] Milton J. Kiefel,[†,▽] John N. A. Hooper,[○] and Anthony R. Carroll[,†,‡]*

[†]School of Environment and Science, Griffith University, Southport, Queensland, 4222, Australia

[‡]Griffith Institute for Drug Discovery, Griffith University, Nathan, Queensland, 4111, Australia

[§]HiLIFE, Institute of Biotechnology, University of Helsinki, Helsinki 00014, Finland

[^]Faculty of Pharmacy, University of Helsinki, Helsinki 00014, Finland

[∥]Discovery Biology, Griffith University, Nathan, Queensland, 4111, Australia

[▽]Institute for Glycomics, Griffith University, Southport, Queensland, 4221, Australia

[○]Queensland Museum, South Brisbane BC, Queensland, 4101, Australia

[*]*Corresponding author. Tel.: +61-7-5552-9187; fax +61-7-5552-7785; E-mail address:* a.carroll@griffith.edu.au

ABSTRACT: Seven new polyaromatic bis-spiroketal-containing butenolides, the prunolides D−I (**4**−**9**) and *cis*-prunolide C (**10**), a new dibrominated β-carboline sulfamate named pityriacitrin C (**11**), alongside the known prunolides A−C (**1**−**3**) were isolated from the Australian colonial ascidian *Synoicum prunum*. The prunolides D−G (**4**−**7**) represent the first asymmetrically brominated prunolides, while *cis*-prunolide C (**10**) is the first reported with a *cis*-configuration about the prunolide's bis-spiroketal core. The prunolides displayed binding activities with the Parkinson's disease-implicated amyloid protein α-synuclein in a mass spectrometry binding assay, while the prunolides (**1**−**5** and **10**) were found to significantly inhibit the aggregation (>89.0 %) of α-synuclein in a ThT amyloid dye assay. The prunolides A−C (**1**−**3**) were also tested for inhibition of pSyn aggregate formation in a primary embryonic mouse midbrain dopamine neuron model with prunolide B (**2**) displaying statistically significant inhibitory activity at 0.5 μM. The antiplasmodial and antibacterial activities of the isolates were also examined with prunolide C (**3**) displaying only weak activity against the 3D7 parasite strain of *Plasmodium falciparum*. Our findings reported herein suggest that the prunolides could provide a novel scaffold for the exploration of future therapeutics aimed at inhibiting amyloid protein aggregation and the treatment of numerous neurodegenerative diseases.

Amyloidosis describes the misfolding and aggregation of proteins and peptides into amyloid fibrils, a phenomena found causal in many incurable neurodegenerative disorders with the second most common being Parkinson's disease (PD).[1,2] Abnormal aggregation and phosphorylation of the 140 amino acid residue synaptic protein α-synuclein (α-syn); resulting in insoluble membranous and proteinaceous intraneuronal inclusions termed Lewy bodies (LBs) and Lewy neurites, is a major histopathological feature observed in the brains of patients with familial and sporadic PD.[1,3-5] Although the exact role of Lewy pathology in PD progression remains unclear, it has been hypothesized to proceed via the α-syn protein aggregation cascade, a process initiated by the misfolding and fibrillization of α-syn and aggregation of amyloid fibrils causing cellular damage, dysfunction and impaired proteostasis that ultimately lead to neuronal cell death.[6,7] Use of novel models, such as pre-formed fibril (PFF)-induced LB-like α-syn aggregation, enables mimicry of LB pathology in cultured dopamine which are one of the most vulnerable neuron population in PD.[4,7,8] Inhibition of the α-syn protein aggregation cascade from soluble monomers to neuro-toxic insoluble forms remains an important target for small molecule therapeutic intervention and the potential treatment of PD and other amyloid protein diseases.[1,9,10]

The marine environment remains a rich source of potential drug leads with marine invertebrates producing diverse secondary metabolites that occupy a chemical space similar to FDA-approved small molecule drugs.[11] Ascidians, synonymously known as tunicates, are a good source of structurally unique and bioactive natural products. Of the 15 approved marine drugs, three ascidian-derived or inspired compounds; lurbinectedin (Zepzelca), trabectedin (Yondelis) and plitidepsin (Aplidin), have been prescribed for the treatment of various cancers.[12] Recently, it has been shown that plitidepsin also has potent antiviral activity against SARS-CoV-2 that is 27.5 times greater than the current standard of care antiviral treatment remdesivir,[13] and is currently undergoing phase 3 clinical trials.[12] Ascidians, in particular those belonging to the

genus *Synoicum*, have also been found to produce bioactive non-nitrogenous polyaromatic butenolide natural products,[14] a structure class that includes rubrolides,[15-19] cadiolides,[20-21] procerolides[22] and the dimeric prunolides.[23] The prunolides, tetraphenolic bis-spiroketal compounds containing a rare 1,6,8-trioxadispiro[4.1.4.2]trideca-3,10,12-triene-2,9-dione carbon structure, have only so far been reported from *Synoicum* species,[17, 19] with a sample of the Australian colonial ascidian *Synoicum prunum* (Herdman, 1899) affording the weakly cytotoxic prunolides A−C (**1**−**3**).[23]

A larger recollection of *S. prunum* has now allowed us to investigate the minor components present in this invertebrate. Furthermore, we report the isolation of eight new and three known marine natural products from *S. prunum* and their biological evaluation against the PD amyloid protein α-syn, the 3D7 parasite strain of *Plasmodium falciparum*, and methicillin-sensitive and resistant *Staphylococcus aureus*.

RESULTS AND DISCUSSION

Following the exhaustive MeOH extraction of a freeze-dried and ground sample of *S. prunum* and extensive HPLC purification, seven new prunolides D to I (**4**−**9**), *cis*-prunolide C (**10**) and a new dibrominated sulfamate-containing β-carboline, pityriacitrin C (**11**), were isolated and characterised by 1D and 2D NMR and MS analysis. Furthermore, three known compounds, the prunolides A−C (**1**−**3**) were re-isolated in good quantities and closely matched their NMR spectroscopic and MS experimental data reported in the literature.[23]

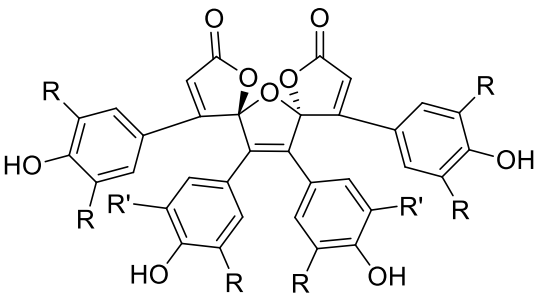

1 R, R' = Br
2 R = Br, R' = H
3 R, R' = H

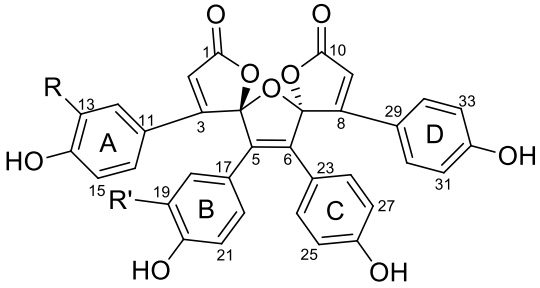

4 R = Br, R' = H
5 R = H, R' = Br

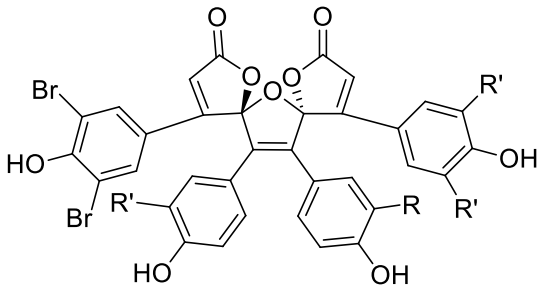

6 R = Br, R' = H
7 R = H, R' = Br

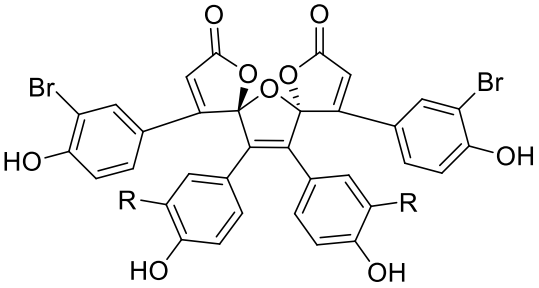

8 R = Br
9 R = H

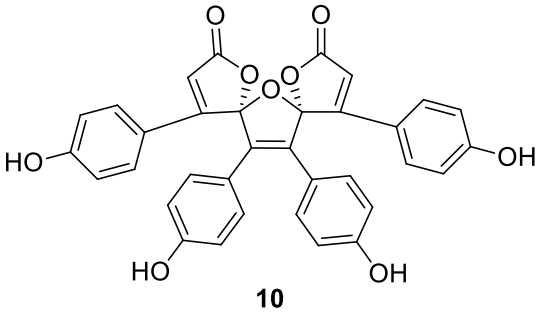

10

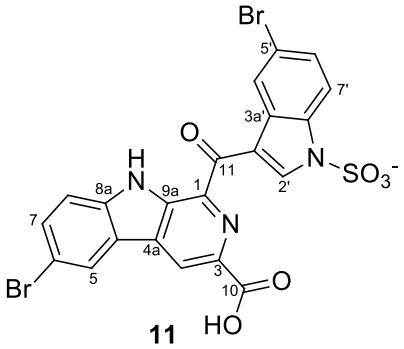

11

Prunolide D (**4**, 1.2 mg) presented as a pale yellow amorphous solid with (-) HRESIMS data displaying a 1:1 deprotonated molecule at *m/z* 651.0288 and 653.0278, consistent with a structure containing one bromine atom and establishing its molecular formula as $C_{34}H_{21}BrO_9$. The ^{1}H NMR data for **4** (Table 1) displayed two olefinic methine singlets (δ_H 6.47 and 6.56) and nine aromatic resonances (δ_H 6.625, 2H; 6.630, 2H; 6.87, 2H; 6.957, 2H; 6.963, 2H; 6.97, 1H; 7.77, 1H; 7.82; 2H and 8.15, 1H), with the aromatic signals able to be ascribed to three 1,4-disubstituted and one 1,3,4-trisubstituted phenyl systems. The ^{13}C NMR and HSQC data (Table 1) for **4** contained two deshielded carbonyl carbon resonances (δ_C 171.0 and 170.8), nine protonated aromatic carbon resonances (δ_C 134.7, 131.6, 131.1*, 130.4, 117.3, 116.8 and

116.7*, where * is coincident carbon chemical shifts), two olefinic methine carbons (δ_C 116.6 and 115.3) and 14 nonprotonated carbons resonances (δ_C 163.7, 162.6, 162.4, 159.74, 159.67, 158.8, 139.5, 138.7, 122.9, 122.0, 121.9, 118.72, 118.71 and 111.3). HMBC correlations from the methine singlet proton signal at δ_H 6.56 (H-2) to the more shielded of the two carbonyl carbon resonances at δ_C 170.8 (C-1), an olefinic nonprotonated carbon resonance at δ_C 162.6 (C-3), an aromatic carbon resonance at δ_C 122.9 (C-11) and a non-protonated carbon resonance at δ_C 118.7 (C-4), allowed the assignment of a α, β-unsaturated butenolide system to **4** (Figure 1). A second α,β-unsaturated butenolide was also able to be assigned to **4** with HMBC correlations observed from the methine proton resonance at δ_H 6.47 (H-9) to the most deshielded carbonyl carbon resonance at δ_C 171.0 (C-10), an olefinic carbon resonance at δ_C 163.7 (C-8) and a non-protonated carbon resonance at δ_C 118.7 (C-7).

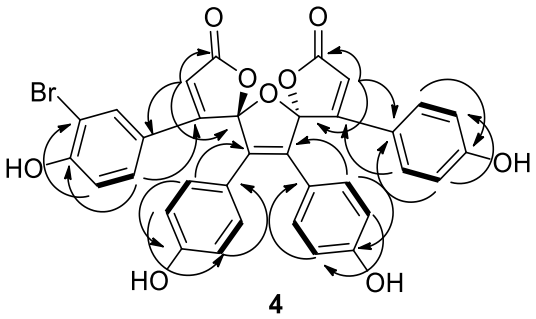

4

Figure 1. Key COSY (bolded lines) and HMBC (arrows) correlations for structure elucidation of prunolide D (**4**).

HMBC correlations (Figure 1) from the desheilded *meta*-coupled proton doublet resonance at δ_H 8.15 (d, 2.2 Hz, H-12) to a phenolic carbon resonance at δ_C 158.8 (C-14), an aromatic methine carbon resonance at δ_C 130.4 (C-16) and a shielded nonprotonated aromatic carbon resonance at δ_C 111.3 (C-13) and a chemical shift consistent with a brominated aromatic carbon *ortho* to an oxygenated aromatic carbon,[17,23] confirmed a 1-substituted-3-bromo-4-phenol in **4** (Figure 1, ring A). Further HMBC correlations between H-12 to δ_C 162.6 (C-3) and H-15 (δ_H

6.97, d, 8.6 Hz, 1H) and δ_C 122.9 (C-11) confirmed the connectivity of the 1-substituted-3-bromo-4-phenol system (ring A) to C-3 of one α,β-unsaturated butenolide moiety. The aforementioned structure assignment was further supported by ROESY correlations from the olefinic butenolide proton resonance at δ_H 6.56 (H-2) to aromatic proton resonances at H-12 (δ_H 8.15) and H-16 (δ_H 7.77) of the 3-bromo-4-phenol system (ring A, Figure 2). Similarly, the connectivity of the second butenolide system was assigned to the most deshielded of the three 1-substituted 4-phenol systems (ring D) in **4** with HMBC correlations from δ_H 7.82 (d, 8.8 Hz, 2H) to the olefinic nonprotonated carbon signal at C-8 (δ_C 163.7). This assignment was also corroborated by ROESY correlations from the olefinic proton resonance at δ_H 6.47 (H-9) to the 1-substituted-4-phenol systems deshielded aromatic proton signal at δ_H 7.82 (H-30 and 34) of ring D.

The remaining two almost coincident 1,4-disubstituted aromatic systems in **4** were confirmed as 1-substituted 4-phenols with HMBC correlations from the *ortho*-coupled aromatic proton resonances of ring B at δ_H 6.693 (H-18 and 22) and ring C at δ_H 6.957 (H-24 and 28) to a coincident oxygenated aromatic carbon resonance at δ_C 159.7* (C-20 and 26) and coincident protonated aromatic carbon resonances at δ_C 131.1*(C-18, 22, 24 and 28). The connectivity of the two phenols (rings B and C) was confirmed by HMBC correlations between δ_H 6.963 (H-18 and 22) and δ_H 6.957 (H-24 and 28) with non-protonated olefinic carbon resonances at δ_C 139.5 (C-5) and δ_C 138.7 (C-6), respectively. Unfulfilled valence requirements remained at four non-protonated carbons; C-4 (δ_C 118.7*), C-5 (δ_C 139.5), C-6 (δ_C 138.7) and C-7 (δ_C 118.7*), alongside three oxygens and one degree of unsaturation from the molecular formula to finalise the structure assignment of **4**. The carbon chemical shifts at C-4 and C-7 (δ_C 118.7*) were consistent with that reported for other hemiketal carbons[23] allowing an assumption of bonds between C-4/C-5 and C-5/C-7; alongside oxygen bridges between C-1 and 4, and C-7 and 10, respectively. The connectivity of rings B and C to olefinic carbons at C-5 and C-6 was

congruent with the assignment of an furan system linking the bis-spiroketal core of **4** via an oxygen bridge between C-4 and C-7, a structural feature consistent with that reported for the prunolides A to C (**1**−**3**).[23] Analysis of ROESY NMR data established the final connectivity of **1** with correlations observed from ring A's H-16 (δ_H 7.77) to ring B's H-18 and 22 (δ_H 6.963), and from ring D's H-30 and 34 (δ_H 7.82) to ring C's H-20 and 28 (δ_H 6.957).

The structure elucidations of the prunolides E−I (**5**−**9**) were accomplished in a similar manner to **4**, relying on thorough analysis of 1D and 2D NMR spectroscopic, and MS spectrometric data. The (-) HRESIMS data for prunolide E (**5**, 1.0 mg, yellow amorphous solid) displayed a 1:1 deprotonated molecule at *m/z* 651.0283 and 653.0274 consistent with the same molecular formula, $C_{34}H_{21}BrO_9$, previously assigned to **4**. The 1D and 2D NMR spectroscopic and MS spectrometric data for **5** suggested that its structure also contained three 1-substituted 4-phenols and a 1-substituted-3-bromo-4-phenol system like **4**, however, differences in connectivity were observed. HMBC analysis assigned two of the non-brominated phenols (rings A and D) to distinct α,β-unsaturated butenolides, while the furan core was ascribed to the more-shielded of the three 1-substituted-4-phenols and a 3-bromo-4-phenol (rings B and C). Shared ROESY correlations between the olefinic singlet proton resonance at δ_H 6.52 (H-2) and the slightly more deshielded aromatic proton signal at δ_H 7.84 (H-12 and 16) of one 1-substituted-4-phenol confirmed the connectivity of ring A's butenolide system (Figure 2). The second α,β-unsaturated butenolide was ascribed to the slightly more shielded 4-phenol system (ring D) with ROESY correlations observed from the olefinic proton singlet resonance at δ_H 6.50 (H-9) to the aromatic proton signal at δ_H 7.82 (H-30 and 34). ROESY NMR correlations between the aromatic proton signal at δ_H 7.19 (H-18) of ring B to the most deshielded aromatic proton resonance at δ_H 7.84 (H-12 and 16) of ring A confirmed the structural arrangement of rings A and B. Further ROESY correlations between the aromatic proton resonance at δ_H 6.95 (H-24 and 28) of ring C and the aromatic proton signal at δ_H 7.82 (H-30 and 34) of ring D finalised

the connectivity of **5**'s phenyl groups. Prunolide E (**5**) can therefore be assigned as a structural isomer of prunolide D (**4**) with the former's 3-bromo-4-phenol system assigned to ring B instead of ring A in **4**.

Prunolide F (**6**) was obtained as a yellow amorphous solid (1.0 mg) with (-) HRESIMS data displaying a 1:3:3:1 deprotonated molecule at *m/z* 806.8497, 808.8471, 810.8458 and 812.8488 consistent with a structure containing three bromine atoms and the molecular formula $C_{34}H_{19}Br_3O_9$. The ^{1}H and ^{13}C NMR data for **6** further confirmed the asymmetry deduced from its molecular formula with two distinct α,β-unsaturated butenolide systems able to be identified. The 1D and 2D NMR spectroscopic data for **6** (Table 1) enabled the assignment of one 1-substituted-3,5-dibromo-4-phenol (ring A), two 1-substituted-4-phenols (rings C and D) and a 1-substituted-3-bromo-4-phenol (ring B) to its structure. The connectivity of ring A to one α,β-unsaturated butenolide system was confirmed by ROESY correlations from the more deshielded of the two olefinic proton resonances at δ_H 6.52 (H-2) to the aromatic singlet proton resonance at δ_H 8.08 (H-12 and 16) of ring A (Figure 2). The second butenolide system in **6** was assigned to ring D with ROESY correlations between the second olefinic singlet resonance at δ_H 6.48 (H-9) and the aromatic doublet proton signal at δ_H 7.82 (H-30 and 34) of ring D, thereby confirming the connectivity assigned from HMBC data. Finally, ROESY correlations from the aromatic proton signal at δ_H 7.82 (H-30 and 34) of ring D were observed to ring C's aromatic doublet proton resonance at δ_H 6.92 (H-28) finalising the connectivity proposed for prunolide F (**6**).

Table 1. NMR Spectroscopic Data for Prunolide D−F (**4**−**6**) (500 MHz, MeOH-d_4) and Prunolide G (**7**) (800 MHz, MeOH-d_4)

	prunolide D (**4**)		prunolide E (**5**)		prunolide F (**6**)		prunolide G (**7**)	
	δ_C[a], type	δ_H, mult (*J* in Hz)	δ_C[a], type	δ_H, mult (*J* in Hz)	δ_C[a], type	δ_H, mult (*J* in Hz)	δ_C[b], type	δ_H, mult (*J* in Hz)
1	170.8, C	-	171.0/171.1, C	-	170.8, C	-	169.8/169.7, C	-
2	116.7, CH	6.56, s	115.3*, CH	6.52, s	115.3, CH	6.52, s	117.8*, CH	6.62, s
3	162.6, C	-	163.8, C	-	161.7, C	-	160.5/160.4, C	-
4	118.7*, C	-	118.6, C	-	118.4*, C	-	118.2/118.1, C	-
5	139.5, C	-	137.6, C	-	139.9, C	-	137.8, C	-
6	138.7, C	-	140.2, C	-	138.2, C	-	140.4, C	-
7	118.7*, C	-	118.7, C	-	118.4*, C	-	118.2/118.1, C	-
8	163.7, C	-	163.9, C	-	163.2, C	-	160.5/160.4, C	-
9	115.3, CH	6.47, s	115.3*, CH	6.50, s	115.6, CH	6.48, s	117.8*, CH	6.61, s
10	171.0, C	-	171.0/171.1, C	-	170.5, C	-	169.8/169.7, C	-
11	122.9, C	-	121.6, C	-	121.4*, C	-	123.1/123.0, C	-
12	134.7, CH	8.15, d (2.2)	131.7, CH	7.84, d (8.8)	133.6, CH	8.08, s	133.5*, CH	8.08, s

13	111.3, C	-	116.8, CH	6.88 (d, 8.8, 1H)	113.9, C	-	112.8/112.7, C	-
14	158.8, C	-	162.5*, C	-	160.0*, C	-	156.5/156.4, C	-
15	117.3, CH	6.97, d (8.6)	116.8, CH	6.88, d (8.8)	113.9, C	-	112.8/112.7, C	-
16	130.4, CH	7.77, dd (8.6, 2.2)	131.7, CH	7.84, d (8.8)	133.6, CH	8.08, s	133.5*, CH	8.08, s
17	122.1/122.0, C	-	123.7, C	-	118.4*, C	-	123.2*, C	-
18	131.1*, CH	6.963, d (8.8)	134.2, CH	7.19, d (2.1)	131.0, CH	6.97, d (8.8)	134.2, CH	7.24, d (2.2)
19	116.7*, CH	6.630, d (8.8)	111.0, C	-	116.8, CH	6.66, d (8.8)	111.3, C	-
20	159.7*, C	-	156.5, C	-	160.0*, C	-	156.7, C	-
21	116.7*, CH	6.630, d (8.8)	117.3, CH	6.72, d (8.5)	116.8, CH	6.66, d (8.8)	117.5, CH	6.76, d (8.5)
22	131.1*, CH	6.963, d (8.8)	130.3, CH	6.89*, obs.	131.0, CH	6.97, d (8.8)	130.0, CH	6.90, dd (8.5, 2.2)
23	122.1/122.0, C	-	121.4*, C	-	123.7, C	-	121.2, C	-
24	131.1*, CH	6.957, d (8.8)	131.1, CH	6.95, d (8.8)	117.4, CH	6.74, d (8.4)	131.0, CH	6.98, d (8.8)
25	116.7*, CH	6.625, d (8.8)	116.8, CH	6.65, d (8.8)	130.2, CH	6.92, dd (8.4, 2.1)	117.0, CH	6.68, d (8.8)
26	159.7*, C	-	159.9, C	-	156.5, C	-	160.1, C	-
27	116.7*, CH	6.625, d (8.8)	116.8, CH	6.65, d (8.8)	111.2, C	-	117.0, CH	6.68, d (8.8)

28	131.1*, CH	6.957, d (8.8)	131.1, CH	6.95, d (8.8)	134.3, CH	7.22, d (2.1)	131.0, CH	6.98, d (8.8)
29	121.4, C	-	121.4*, C	-	121.4*, C	-	123.1/123.0, C	-
30	131.6, CH	7.82, d (8.8)	131.7, CH	7.82, d (8.8)	131.6, CH	7.82, d (8.7)	133.5*, CH	8.07, s
31	116.8, CH	6.87, d (8.8)	116.8, CH	6.89, d (8.8)	116.9, CH	6.89, d (8.7)	112.8/112.7, C	-
32	162.4, C	-	162.5*, C	-	162.4, C	-	156.5/156.4, C	-
33	116.8, CH	6.87, d (8.8)	116.8, CH	6.89, d (8.8)	116.9, CH	6.89, d (8.7)	112.8/112.7, C	-
34	131.6, CH	7.82, d (8.8)	131.7, CH	7.82, d (8.8)	131.6, CH	7.82, d (8.7)	133.5*, CH	8.07, s

[a]125 MHz, [b]201 MHz, *coincident carbon or proton chemical shift.

Prunolide G (**7**) presented as a yellow amorphous solid (1.1 mg) with (-) HRESIMS data displaying a 1:5:10:10:5:1 deprotonated molecule at *m/z* 962.6711, 964.6692, 966.6663, 968.6646, 970.6638 and 972.6643 consistent with a structure containing five bromine atoms and establishing the molecular formula $C_{34}H_{17}Br_5O_9$. The 1D and 2D NMR spectroscopic data for **7** contained two distinct α, β-unsaturated butenolide systems assigned to each of two almost coincident 1-substituted-3,5-dibromo-4-phenols (rings A and D), alongside a 1-substituted-3-bromo-4-phenol and a 1-substituted-4-phenol (rings B and C, respectively). The connectivity of **7** was confirmed by the analysis of ROESY correlations between the slightly more deshielded of the two aromatic proton singlet resonances at δ_H 8.08 (H-12 and 16, ring A) to the olefinic proton signal of one butenolide moiety at δ_H 6.90 (H-2, Figure 2) Furthermore, shared ROESY correlations between δ_H 8.07 (H-30 and 34, ring D) and the second olefinic proton resonance at δ_H 6.90 (H-10) confirmed the connectivity of **7**'s two butenolide systems to rings A and D. The 1-substituted-3-bromo-4-phenol of **7** was assigned next to ring A with ROESY correlations observed between δ_H 8.08 (H-12 and 16) and aromatic proton resonances H-18 and 22 (ring B). This assignment was confirmed by shared ROESY correlations between ring D's singlet proton resonance at δ_H 8.07 (H-30 and 34) and δ_H 6.98 (H-24 and 28) of the 1-substituted-4-phenol in **7**. Prunolide G (**7**) shares dibromophenolic A and D ring systems with the prunolides A and B (**1** and **2**), while the B and C ring systems are the same as those in prunolide B (**2**) and C (**3**) respectively.[23] The prunolides D−G (**4**−**7**) represent the first asymmetrically brominated prunolides isolated and reported in this class.

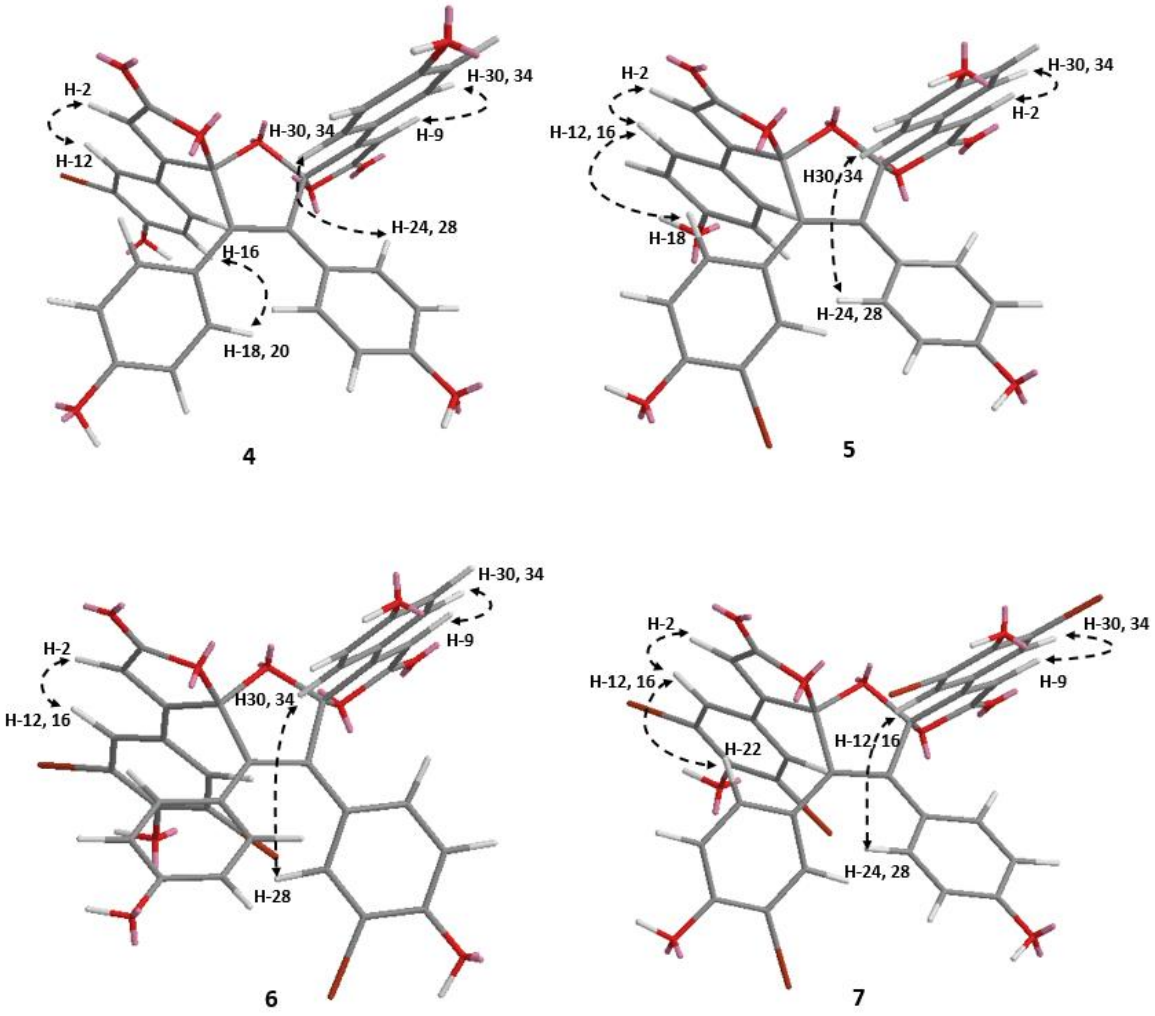

Figure 2. Key ROESY correlations for structure assignment and connectivity of the asymmetric prunolides D−G (**4**−**7**).

Prunolide H (**8**) was isolated as a yellow amorphous solid (1.0 mg) with the (-) HRESIMS data displaying a 1:4:6:4:1 deprotonated molecule at *m/z* 884.7627, 886.7616, 888.7596, 890.7577 and 892.7575 consistent with a compound containing four bromine atoms and the molecular formula $C_{34}H_{18}Br_4O_9$. The ^{1}H and ^{13}C NMR data (Table 2) for **8** suggested it contained an element of symmetry with four 1-substituted-3-bromo-4-phenol systems and two identical α,β-unsaturated butenolides. HMBC correlations confirmed the assignment of two identical 3-bromo-4-phenol (rings A and D) substituted butenolides in **8**, while the more shielded monobrominated phenols (rings B and C) were assigned to the furan core of the prunolide

structure. Prunolide H (**8**) is therefore the A and D ring monobrominated analogue of prunolide B (**2**) with both compounds sharing 1-substituted-3-bromophenolic B and C ring systems.

Table 2. NMR Spectroscopic Data for Prunolide H (**8**) and *cis*-Prunolide C (**10**) (500 MHz, DMSO-d_6) and Prunolide I (**9**) (800 MHz, MeOH-d_4)

position	prunolide H (**8**)		prunolide I (**9**)		*cis*-prunolide C (**10**)	
	δ_c[a], type	δ_H (mult, *J* in Hz)	δ_c[b], type	δ_H (mult, *J* in Hz)	δ_c[a], type	δ_H (mult, *J* in Hz)
1,10	168.2, C	-	170.3, C	-	168.8, C	-
2, 9	115.8, CH	6.93, s	116.7, CH	6.55, s	116.6, CH	6.77, s
3, 8	159.4, C	-	162.2, C	-	161.4, C	-
4, 7	115.9, C	-	118.7, C	-	115.6, C	-
5, 6	136.5, C	-	not obs., C	-	136.5, C	-
11	120.5, C	-	123.1, C	-	119.7, C	-
12	133.0, CH	8.12, d (2.3)	134.3, CH	8.14, d (2.3)	130.2, CH	7.44, d (8.7)
13	110.3, C	-	111.2, C	-	115.9*, CH	6.72, d (8.7)
14	158.9, C	-	159.3, C	-	160.6, C	-
15	116.8, CH	7.03, d (8.6)	117.2, CH	6.97, d (8.7)	115.9*, CH	6.72, d (8.7)
16	129.3, CH	7.75, dd (8.6, 2.3)	130.2, CH	7.76, dd (8.7, 2.3)	130.2, CH	7.44, d (8.7)
17	120.9, C	-	122.0, C	-	120.5, C	-
18	132.2, CH	7.19, d (2.2)	130.8, CH	6.97, d (8.8)	129.7, CH	6.95, d (8.7)
19	109.8, C	-	116.4, CH	6.64, d (8.8)	115.9*, CH	6.67, d (8.7)
20	155.4, C	-	159.8, C	-	158.2, C	-
21	117.0, CH	6.88, d (8.5, 2.2)	116.4, CH	6.64, d (8.8)	115.9*, CH	6.67, d (8.7)
22	128.8, CH	6.91, dd (8.6, 2.3)	130.8, CH	6.97, d (8.8)	129.7, CH	6.95, d (8.7)

23	120.9, C	-	122.0, C	-	120.5, C	
24	128.8, CH	6.91, dd (8.6, 2.3)	130.8, CH	6.97, d (8.8)	129.7, CH	6.95, d (8.7)
25	117.0, CH	6.88, d (8.5, 2.2)	116.4, CH	6.64, d (8.8)	115.9*, CH	6.67, d (8.7)
26	155.4, C	-	159.8, C	-	158.2, C	-
27	109.8, C	-	116.4, CH	6.64, d (8.8)	115.9*, CH	6.67, d (8.7)
28	132.2, CH	7.19, d (2.2)	130.8, CH	6.97, d (8.8)	129.7, CH	6.95, d (8.7)
29	120.5, C	-	123.1, C	-	119.7, C	-
30	129.3, CH	7.75, dd (8.6, 2.3)	130.2, CH	7.76, dd (8.7, 2.3)	130.2, CH	7.44, d (8.7)
31	116.8, CH	7.03, d (8.6)	117.2, CH	6.97, d (8.7)	115.9*, CH	6.72, d (8.7)
32	158.9, C	-	159.3, C	-	160.6, C	-
33	110.3, C	-	111.3, C	-	115.9*, CH	6.72, d (8.7)
34	133.0, CH	8.12, d (2.3)	134.3, CH	8.14, d (2.3)	130.2, CH	7.44, d (8.7)

[a]125 MHz. [b]carbon chemical shifts derived from HSQC and HMBC data measured at 201 MHz.
*coincident carbon chemical shifts

Prunolide I (**9**, yellow amorphous solid, 0.3 mg) displayed a 1:2:1 dibrominated deprotonated molecule in the (-) HRESIMS at *m/z* 728.9475, 730.9375 and 732.9394 indicating a molecular formula $C_{34}H_{20}Br_2O_9$. Like prunolide H (**8**), a plane of symmetry was able to be assigned to **9** by analysis of its 1D and 2D NMR spectroscopic data (Table 2). HMBC correlations enabled the assignment of two identical α,β-unsaturated butenolide systems attached to two 1-substituted-3-bromo-4-phenols (rings A and D) and two 1-substituted-4-phenols (rings B and C) were ascribed to **9**'s furan core. The prunolides D−I (**4**–**9**) were all able to be assigned *trans*-configuration about their bis-spiroketal cores with reference to the NMR and X-ray crystallographic data reported by Carroll et al. for the known prunolides A−C (**1**−**3**).[23] The relative configuration of prunolides D (**4**) and E (**5**) was assigned *trans* upon comparison with

the NMR data reported for prunolide C (**3**) and its 1,4-disubstituted A and D phenyl systems.[23] Prunolides F (**6**) and G (**7**) were compared with the NMR data reported for both, prunolide A and B's (**1-2**) dibrominated phenol systems, as well as prunolide C's (**3**) non-brominated phenol for **6**. [23] The monobrominated A and D phenols of prunolides H (**8**) and I (**9**) were consistent with the NMR data obtained for prunolide D (**4**).

The *cis*-isomer of prunolide C (**10**) presented as a yellow amorphous solid (1.2 mg) with (-) HRESIMS data displaying a deprotonated molecule at *m/z* 573.1201 allowing for the molecular formula $C_{34}H_{22}O_9$, identical to that reported for the known compound prunolide C (**3**).[23] The ^{1}H and ^{13}C NMR data (Table 2) suggested **10** contained a plane of symmetry with two identical α,β-unsaturated butenolide systems and four 1-substituted-4-phenols able to be assigned. Analysis of HMBC spectroscopic data for **10** confirmed that the two deshielded 1-substituted-4-phenols (rings A and D) were attached to the unsaturated non-protonated carbons (C-3 and C-8) associated with symmetrical butenolide systems, while the more shielded phenols (rings B and C) were ascribed to the furan system of the prunolide structure. While the MS spectrometric data for **10** was identical to that reported for prunolide C (**3**),[23] distinct chemical shift differences present in the ^{1}H NMR spectra for **10** indicated that it must be isomeric with **3**.

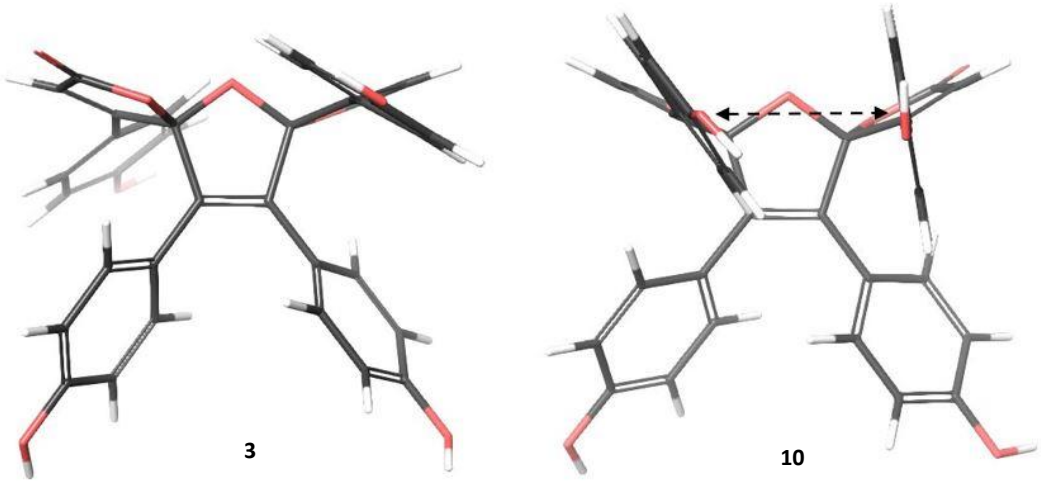

Figure 3. MCMM (OPLS3 forcefield) lowest energy conformers of prunolide C (**3**) and *cis*-prunolide C (**10**) highlighting the anisotropic shielding effects caused by the relative closeness in space of **10**'s aromatic systems due to its *cis*-configuration across the bis-spiroketal.

Comparatively, the aromatic proton resonances at δ_H 7.44 (H-12, 16, 30 and 34) and δ_H 6.72 (H-13, 15, 31 and 33) of the 1,4-disubstituted A and D phenyl systems of **10** were more shielded (0.37 ppm and 0.14 ppm, respectively) than those reported for prunolide C (**3**).[23] Furthermore, the ^{1}H NMR chemical shifts of **10**'s B and C ring systems aromatic protons remained consistent with those reported for prunolide C (**3**) suggesting that differences between the two compounds must reside within the relative configuration associated with the structure's bis-spiroketal core. The shielding effects observed in the ^{1}H NMR resonances for **10** would likely be due to anisotropic effects attributed to the in-space proximity of rings A and D due to the *cis* configuration across the bis-spiro ketal core (Figure 3). The differences observed in the NMR spectra for both compounds were supported by differing preparative RP HPLC retention times with *cis*-prunolide C (**10**) eluting in the slightly more polar fractions than prunolide C (**3**). This finding supports the proposal made by Sofikiti et al. during their synthesis of the prunolide spirocyclic core that the difference in polarity is likely due to the directional differences in dipole alignment between the *cis* (same direction) and *trans* (opposing directions) butenolide

systems.[24] The isolation of *cis*-prunolide C (**10**) is the first reported compound in this class with a *cis* configuration about its bis-spiroketal core.

The optical rotation (OR) data obtained for the prunolides **4**−**9** displayed negligible positive specific rotations suggesting their isolation as racemates. Exploratory experimental ECD spectra were acquired for two prunolide samples, prunolides D (**4**) and E (**5**), however, both displayed relatively flat ECD spectra consistent with that of racemic mixtures. These findings support the optical rotation data reported for the prunolides A−C (**1**−**3**) during their original isolation by Carroll et al.,[23] and observations made by Sofikiti et al. for the synthesis of the prunolide core.[24]

Pityriacitrin C (**11**) was isolated as a brown amorphous solid (0.7 mg) with the (-) HREISMS data displaying a dibrominated deprotonated molecule at *m/z* 589.8660, 591.8634 and 593.8624 consistent with the molecular formula $C_{21}H_{11}Br_2N_3O_6S$. The ^{1}H NMR spectrum for **11** displayed eight deshielded proton resonances including a broad singlet at δ_H 12.5 (NH-9, 1H), two aromatic singlets at δ_H 9.82 (H-2', 1H) and δ_H 9.22 (H-4, 1H), two *meta* coupled aromatic doublets at δ_H 8.76 and 8.75 (H-5 and H-4', 2H), two *ortho* coupled aromatic doublet signals at δ_H 7.90 (H-7', 1H) and 7.83 (H-8, 1H) and two *ortho* and *meta* coupled aromatic doublet of doublet resonances at δ_H 7.77 (H-7) and 7.49 (H-6') (Table 3). The ^{13}C NMR and HSQC data for **11** established two carbonyl carbon resonances; one consistent with a biaryl ketone at δ_C 186.6 (C-11) and the other a carboxylic acid at δ_C 166.6 (C-10), eight aromatic methine groups (δ_C 140.3*, C-2'; 131.7, C-7; 125.7, C-6'; 123.9, C-5; 124.9, C-4'; 120.7, C-4; 116.2, C-7' and 115.4, C-8, where * refers to coincident carbon chemical shifts), and 11 non-protonated carbon resonances (δ_C 140.8, C-8a; 140.3*, C-1; 136.2, C-9a; 133.4, C-7a'; 133.4, C-1; 129.9, C-3a'; 130.4, C-4a; 122.5, C-4b; 112.9, C-6; 115.6, C-5′ and 111.9, C-3'). Notably, the broad proton singlet resonance at δ_H 12.51 (H-9) did not display a HSQC correlation and its deshielded chemical shift suggested that it was likely attached to a

heteroaromatic nitrogen, presumably the nitrogen of an indole system. HMBC correlations from the deshielded proton at δ_H 12.51 (H-9) to nonprotonated carbons at 140.3* (C-1), δ_C 130.4 (4a), 122.5 (C-4b) and 136.2 (C-9a) supported the presence of a C-2 and C-3 substituted indole system (Figure 4). Moreover, HMBC correlations from the aromatic singlet resonance at δ_H 9.22 (H-4) to carbons at C-4b (δ_C 122.5), C-9a (δ_C 136.2), and to a carbonyl carbon signal consistent with a carboxylic acid at δ_C 166.6 (C-10) allowed the assignment of a 1-substituted β-carboline with a carboxylic acid substituted C-3 position. Mutual aromatic coupling constants between δ_H 8.75 (H-5), 7.77 (H-7) and 7.83 (H-8), alongside HMBC correlations to nonprotonated aromatic carbons C-4b (δ_C 122.5) and C-8a (δ_C 140.8), and to a shielded aromatic carbon resonance consistent with attachment to bromine at δ_C 112.9 (H-6), confirmed the assignment of a 1-substituted 6-bromo-3-carboxylic acid-β-carboline to **11**.

Table 3. NMR Spectroscopic Data (800 MHz, DMSO-d_6) for Pityriacitrin C (**11**)

	pityriacitrin C (**11**)		
	δ_C[a], type	δ_H, mult (*J* in Hz)	HMBC[b]
1	140.3*, C	-	-
2-N	-	-	-
3	136.9, C	-	-
4	120.7, CH	9.22, br s	3, 4b, 9a, 10
4a	130.4, C	-	-
4b	122.5, C	-	-
5	123.9, CH	8.75, d (2.0)	6, 7, 8a
6	112.9, C	-	-
7	131.7, CH	7.77, dd (8.7, 2.0)	5, 6, 8a
8	115.4, CH	7.83, d (8.7)	4b, 6
8a	140.8, C	-	-
9-NH	-	12.51, br s	1, 4a, 4b, 9a
9a	136.2, C	-	-
10	166.6, C	-	-
11	186.6, C	-	-
1′-NSO_3H	-	-	-
2′	140.3*, CH	9.82, s	3’, 3a’, 7a’
3′	111.9, C	-	-
3a′	129.9, C	-	-
4′	124.9, CH	8.76, d (2.0)	5’, 6’, 7a’
5′	115.6, C	-	-
6′	125.7, CH	7.49, dd (8.6, 2.0)	4’, 5’, 7a’
7′	116.2, CH	7.90, d (8.6)	3a, 5
7a′	133.4, C	-	-

[a]201 MHz, [b]HMBC correlations are from the proton(s) stated to the indicated carbon, *coincident proton and carbon chemical shift

Similarly, a second brominated aromatic system was ascribed to **11** by analysis of HMBC correlations from H-7′ (δ_H 7.90) to a quaternary aromatic carbon at δ_C 129.9 (C-3a′) and a brominated aromatic carbon resonance at δ_C 115.6 (C-5′). Further HMBC correlations from the aromatic proton resonances at H-4′ (δ_H 8.76 to carbons at δ_C 115.6 (C-5′), 125.7 (C-6′) and 133.4 (C-7a′), and from H-6′ (δ_H 7.49) to carbon signals at δ_C 124.9 (C-4′), 115.6 (C-5′) and 133.4 (C-7a′), confirmed the assignment of a second 4-bromo-1,2-substituted aromatic system to **11**. HMBC correlations from δ_H 9.82 (H-2′) to non-protonated aromatic carbon resonances at δ_C 111.9 (C-3′), 129.9 (C-3a′) and 133.4 (C-7a′), coupled with the absence of a second indole

proton in the ^{1}H NMR spectrum, suggested the 4-brominated-1,2-substituted aromatic moiety was in fact a 1,3-disubstituted-5-bromoindole.

All that remained for finalizing the structure of **11** were unfulfilled valence requirements at C-1 (δ_C 140.3*) and C-3′ (δ_C 111.9), one carbonyl carbon at δ_C 186.6 (C-11), and 80 mass units from the HRESIMS data. The chemical shift of C-11 (δ_C 186.6) was consistent with that reported for a bisaryl ketone bridging the brominated β-carboline and 5-bromoindole systems between C-1 and 3′, respectively.[25] This assignment was supported by the deshielded chemical shift observed for H-2′ (δ_H 9.82); assigned *ortho* to the ketone bridge at C-3′ , which was likely due to its close location in-space to the ketone at C-11.[25] The remaining 80 mass units from **11**'s molecular formula was assigned to a sulfonic acid attached to the indole nitrogen at N-1′ that formed part of an indole sulfamate group.

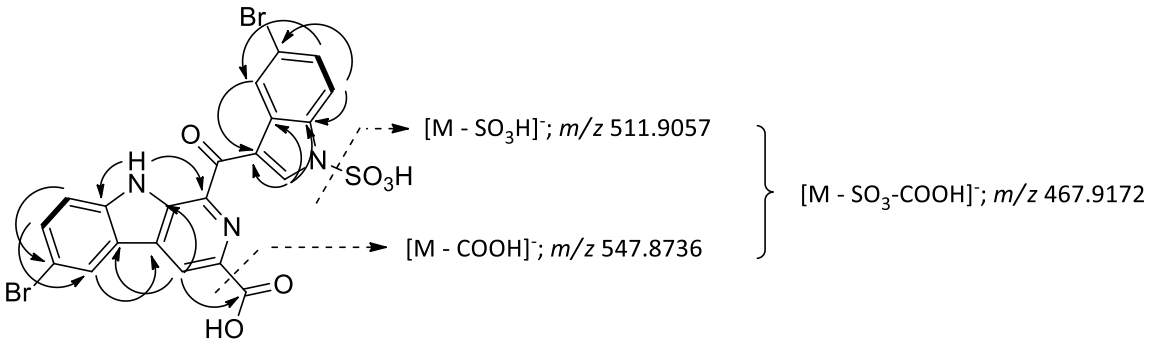

Figure 4. Key COSY (bolded lines) and HMBC (solid arrows) correlations and targeted (-) HRESIMS MS/MS fragmentation (dashed arrows) of pityriacitrin C (**11**).

The assignment of an indole sulfamate to **11** was corroborated by targeted MS/MS fragmentation that upon increasing cone voltage displayed the facile loss of 80 amu from the **11**'s protonated molecule consistent with the loss of SO_3 from the indole nitrogen (Figure 4).[25,26] Moreover, at the highest cone voltage (100 eV) both the sulfonic and carboxylic acid groups were liberated from the molecule with the $[M\text{-}H^{+}\text{-}SO_3\text{-}COOH]^{-}$ ion at *m/z* 467 displayed in the HRMS spectrum. The dibrominated β-carboline sulfamate structure assigned to **11** is closely related to pityriacitrin and pityriacitrin B, both isolated from the pathogenic yeast

Malassezia furfur,[27,28] and is one of only 11 indole sulfamate-containing marine natural products reported in the MarinLit database (2019).[29]

The prunolides (**1**−**10**) were evaluated for α-syn binding activity using an *in vitro* mass spectrometry (MS) assay. The prunolides were incubated with α-syn at a 5:1 ratio for 3 h, after which a (+) HRESIMS spectrum was acquired (Figure 5). The MS binding assay results showed that all of the prunolides formed protein-ligand complexes with α-syn (Table 4), with the exception of **9** which upon NMR analysis was found to have degraded. To evaluate if the observed binding of the compounds with α-syn translated into anti-aggregation activity, the prunolides A−E (**1**−**5**) and c*is*-prunolide C (**10**) were incubated with α-syn at 1:1 and 5:1 (compound:protein) molar ratios for 36 h under conditions that promote amyloid aggregation. The fluorescence thioflavin T (ThT) was used to quantify the presence of amyloid aggregates during the protein aggregation process.

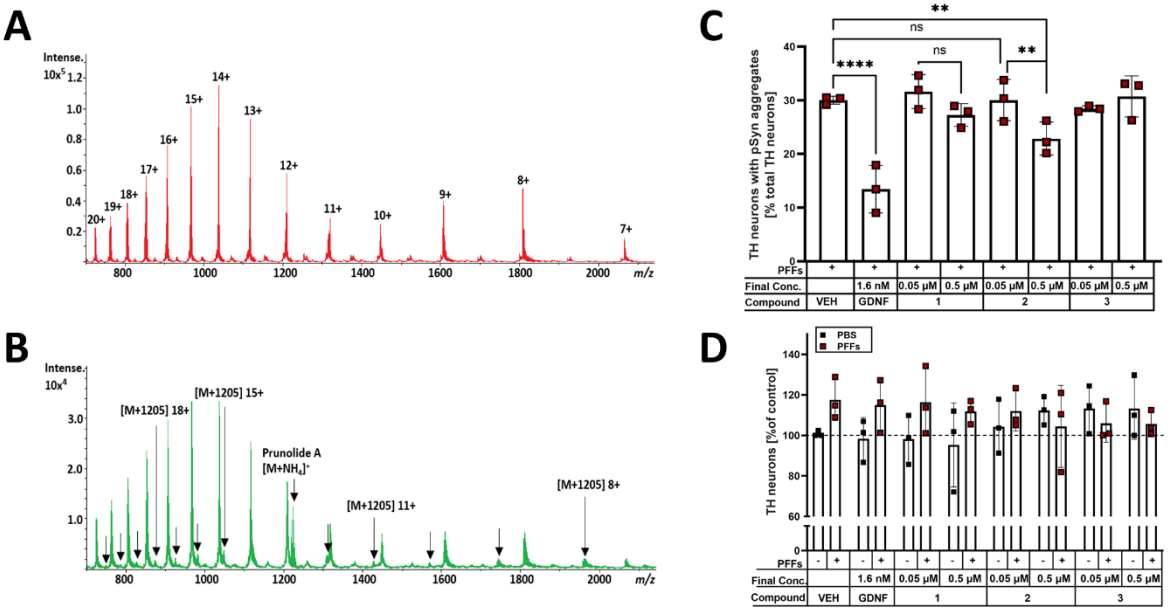

Figure 5. α-synuclein (α-syn) MS binding assay spectra for prunolide A (**1**) and dose dependent effect of prunolide B (**2**) treatment on phosphorylated-serine 129-α-synuclein (pSyn) aggregation in primary embryonic mouse midbrain dopamine neurons. (**A**) Untreated α-syn with peaks marked by charged state of protein. (**B**) α-syn treated with prunolide A (**1**), with arrows indicating α-syn-prunolide A (**1**) protein-ligand complex. (**C**) Compared to vehicle (VEH) control, numbers of tyrosine hydroxylase (TH) positive neurons containing pSyn aggregates were significantly reduced by treatment with 0.5 μM prunolide B (**2**) (**p<0.01);

this effect was not present at the lowest dose (0.05 µM). Prunolides A (**1**) and C (**3**) did not show any effect on numbers of pSyn aggregate containing TH neurons. Treatment with 1.6 nM GDNF was used as a positive control (****p<0.0001) (one-way ANOVA, followed by two-stage linear step-up procedure of Benjamini, Krieger and Yekutieli).[30] (**D**) None of the compounds (**1**−**3**), in combination with PFFs or not, caused statistically significant changes in numbers of TH neurons at 0.05 and 0.5 μM (two-way ANOVA, followed by two-stage linear step-up procedure of Benjamini, Krieger and Yekutieli).[30] N=3 independent experiments, all data are mean ± SD.

The addition of the prunolides (**1**−**5** and **10**) reduced the fluorescence of ThT indicating direct inhibition of α-syn aggregation (Table 4). It was observed that at the 1:1 molar ratio prunolide C (**3**) inhibited aggregation of α-syn more strongly than its brominated analogues. However, at the 5:1 molar ratio the brominated prunolides (**1**, **2**, **4** and **5**) all displayed greater inhibition of protein aggregation than **3** suggesting that the solubility of the larger brominated analogues significantly impacted their inhibitory activities at the 1:1 molar ratio. Interestingly, prunolide C (**3**) also displayed stronger inhibitory activities than *cis*-prunolide C (**10**) at both concentrations tested, suggesting that *trans* configuration about the bis-spiroketal of the prunolides is favorable for anti-aggregation activity. The prunolides A−C (**1**−**3**) were also tested in a primary embryonic mouse midbrain model containing tyrosine hydroxylase (TH) positive dopamine neurons treated with pre-formed fibrils (PFF).[4] Compared to VEH control, prunolide B (**2**) was found to significantly reduce the number of TH-positive dopamine neurons containing phosphorylated-serine 129-α-syn (pSyn) aggregates at 0.5 μM, while **1** and **3** showed little effect at the concentration tested (Figure 5C). The prunolides A−C (**1**−**3**) were also found to have no statistically significant toxic effects on TH-positive dopamine neurons at 0.5 μM compared with controls (Figure 5D). The TH-neuron pSyn results for prunolide B (**2**) supports the likelihood that solubility issues affect the crossing of cell membranes with no effect on the inhibition of pSyn aggregates observed at 0.05 μM.

Table 4. α-synuclein MS binding assay and inhibition of aggregation activities for prunolides (**1**−**10**).

Compound	binding	% inhibition[a]			
	Yes/No	% ± SE (1:1 mol ratio)	t_{50} [b]	% ± SE (5:1 mol ratio)	t_{50} [b]
1	Yes	13.3 ± 1.8	10	89.0 ± 1.8	13.7
2	Yes	34.3 ± 3.7	9.4	99.9 ± 0.0	10
3	Yes	60.0 ± 1.8	6.2	75.2 ± 3.4	14.5
4	Yes	39.0 ± 5.0	1	97.6 ± 0.2	4
5	Yes	24.9 ± 5.6	2	92.9 ± 5.6	4
6	Yes	-	-	-	-
7	Yes	-	-	-	-
8	Yes	-	-	-	-
9	n.a *	-	-	-	-
10	Yes	22.1 ± 3.8	0	51.5 ± 2.5	2.3
ECGC	Yes	90.9 ± 2.6	9.4	98.9 ± 0.5	11.1

[a] Measured as the change in fluorescence of the amyloid dye ThT at the end of the aggregation reaction relative to the negative control; [b] t_{50} corresponds to the difference in h between the midpoint of the aggregation reaction in the presence and absence of the compounds, *compound degraded, - not tested.

The antibacterial activities of the prunolides A−G (**1**−**7**) and *cis*-prunolide C (**10**) were explored against Gram-positive methicillin-sensitive and methicillin-resistant *Staphylococcus aureus* (Table S1). While prunolide E (**5**) and G (**7**) both demonstrated the strongest activities against MSSA (IC_{50} 10.8 and 12.2 μM, respectively) and MRSA (IC_{50} 16.1 and 11.6 μM, respectively), all of the tested were considered inactive (IC_{50} >10 μM). Interestingly, the non-brominated prunolides **3** and **10** were inactive at the highest dose tested suggesting that bromination is important for antibacterial activity. Furthermore, prunolide E (**5**) displayed a two-fold increase in activity against both *S. aureus* strains compared with prunolide D (**4**) indicating that monobromination of the B-ring was more favourable than the A-ring system. The antibacterial results reported for **5** and **7** herein are consistent with that recently reported for rubrolide A against MSSA (MIC 13.4 μM).[15]

Finally, the prunolides A−C (**1**−**3**) and pityriacitrin C (**11**) were tested for antiplasmodial activity against the *Plasmodium falciparum* 3D7 strain, with prunolide C (**3**) displaying weak activity at IC_{50} 5.1 μM (SI = 7.6), while pityriacitrin C (**8**, IC_{50} 15.1 μM, SI = 2.66) showed minimal activity (Table S1). All of the compounds tested against *P. falciparum* demonstrated minimal cytotoxic activities against a human embryonic kidney (HEK293) cell line (Table S1). The antiplasmodial and antibacterial activities displayed by the prunolides, alongside trends observed in the α-syn ThT and mouse dopamine neuron pSyn aggregation assays, support the probability that the more brominated prunolides have inherent limitations crossing cell membranes caused by poor solubility.

Polyphenolic compounds have been identified as good structural sources for the rational design and discovery of anti-amyloid drug-leads with natural product inhibitors of amyloidosis, including epigallocatechin-3-gallate, curcumin and resveratrol, proceeding to clinical trials for the treatment of Alzheimer's Disease.[6] Interestingly, the procerolides, butenolide-containing natural products isolated from the Australian ascidian *Polycarpa procera*, displayed potent anti-prion activities in a yeast-based assay and are structurally related to the prunolides.[22] These findings suggest that the prunolides, and other butenolide-containing natural products for that matter, could provide important polyphenolic structural backbones that should be explored for the future development of ascidian-inspired amyloid therapeutics.

In summary, seven new prunolides (**4**−**10**), the known prunolides A−C (**1**−**3**) and a new dibrominated sulfamate-containing β-carboline, pityriacitrin C (**11**), were isolated from the Australian ascidian *S. prunum*. The α-syn binding and aggregation inhibitory activities of the prunolides provide useful new marine natural product structures available for future optimization targeted at the treatment of PD and other neurological diseases caused by the misfolding and aggregation of amyloid proteins.

EXPERIMENTAL SECTION

General Experimental Procedures. Optical rotations were recorded on a JASCO P-1020 polarimeter, UV spectra were recorded on a Shimadzu UV-1800 spectrophotometer. ECD spectra were recorded on a JASCO J-715 spectropolarimeter. One and two-dimensional NMR spectra were recorded at 25 °C on a Bruker Avance III 500 MHz spectrometer (BBFO Smartprobe, 5 mm 31P-109Ag) and/or a Bruker Avance III HDX 800 MHz with a triple (TCl) resonance 5 mm cryoprobe. The ^{1}H and ^{13}C NMR chemical shifts were referenced to the solvent peak for either, DMSO-d_6 at δ_H 2.50 and δ_C 39.52, or MeOH-d_4 at δ_H 3.31 and δ_C 49.00, respectively. High resolution negative electrospray ionization mass measurements were acquired using CH_3CN as the mobile phase on an Agilent Technologies 6530 Accurate-Mass Q-TOF LC/MS with a 1200 Series autosampler and 1290 Infinity HPLC, while low resolution mass measurements were obtained from with a Waters ZQ electrospray ionisation mass spectrometer. A Merck Hitachi L7100 pump equipped with a Merck Hitachi L7455 PDA detector and a Merck Hitachi L7250 autosampler were used for HPLC. Fractions were collected using a Gilson 215 liquid handler. The solvents used for chromatography were Scharlau HPLC grade, and H_2O was Millipore Milli-QPF filtered. Trifluoroacetic acid (TFA) was spectroscopy grade from Alfa Aesar, while solvents used for HRESIMS were MS grade.

Animal Material. *Synoicum prunum* (Herdman, 1899) was collected by SCUBA from Boat Rock, North Stradbroke Island, Queensland, Australia in December 2000. A voucher specimen of the ascidian sample (G317402) was taxonomically identified by John Kennedy and housed at the Queensland Museum.

Extraction and Isolation. The freeze-dried and ground *S. prunum* sample (635.0 g) was extracted exhaustively in MeOH affording a deep brown extract (34.8 g). The extract was fractionated by vacuum liquid chromatography (VLC) using a decreasing polarity stepwise solvent gradient from H_2O to MeOH yielding seven fractions (100% H_2O, 80% H_2O/20%

MeOH, 70% H_2O/30% MeOH, 50% H_2O/50% MeOH, 40% H_2O/60% MeOH, 20% H_2O/80% MeOH and 100% MeOH). The 40% H_2O/60% MeOH, 20% H_2O/80% MeOH and 100% MeOH VLC fractions were combined (3.10 g) and subjected to four identical RP HPLC separations (Fractions A-D). Each fraction was adsorbed onto C_{18} bonded silica gel and loaded into an HPLC pre-column cartridge (10 mm x 20 mm) connected in series to a preparative C_{18}-bonded silica gel RP HPLC column (Betasil C_{18} 5μm 100 Å, 21.2 mm x 150 mm). The column was eluted with a gradient from 100% H_2O (0.1% TFA) to 100% MeOH (0.1% TFA) over 90 min at a flow rate of 9 mL/min with fractions collected each min. with UV-DAD spectroscopic analysis conducted in tandem with the separation (Fractions A−D). Fractions 36−37 of B contained *cis*-prunolide C (**10**, 1.2 mg), fraction 39−41 of B afforded the known compound prunolide C (**3**, 1.4 mg), while fractions 49−52 (fraction 1, 292.3 mg) of A−D, 38−48 B−D (fraction 2, 323.0 mg) and 52−70 (fraction 3, 1.12g) A−D were recombined separately. Fraction 1 (A−D, 293.2 mg) was subjected to further preparative RP HPLC purification (Kinetex EVO C_{18} 5μm 100 Å, 21.2 x 150 mm) using an optimised solvent gradient from 40% H_2O/60% MeOH (0.1% TFA) to 25% H_2O/ 75% MeOH (0.1% TFA) over 70 min. with fractions collected each min. at a flow rate of 9 mL/min, the column was then eluted in 100% MeOH for a further 10 min. with fraction 24 containing prunolide G (**7**, 1.1 mg) and fractions 9−18 (18.6 mg) recombined and further purified by RP HPLC. Fractions 9−18 (18.6 mg) were injected (150μL in MeOH) onto a C_{18} semi-preparative column (SupelCo Inc. Hypersil Phenyl-2, 5μm, 10 x 250 mm) according to an optimised solvent gradient from 62% H_2O/38% MeOH to 35% H_2O/65% MeOH over 75 min. at a flow rate of 4 mL/min with fraction 28 affording prunolide I (**9**, 0.3 mg,). RP isocratic semi-preparative RP HPLC (Betasil $C_{18,}$ 5 μm, 250 x 10 mm) with a flow rate of 4.0 mL/min was performed on combined fractions with hand collected fractions 1 and 2 affording prunolide D (**4**, 1.2 mg) and E (**5**, 1.0 mg), respectively. Fraction 2 (B−D, 323.0 mg) were further purified by RP HPLC (Kinetex EVO C_{18} 5μm 100 Å, 21.2 X 150 mm)

according to a decreasing polarity gradient from 45% H_2O/55% MeOH (0.1% TFA) to 30% H_2O/70% MeOH over 70 min., then to 100% MeOH (0.1% TFA) over 20 min. at a flow rate of 9 mL/min. Fraction 9 afforded prunolide C (**3**, 1.5 mg), while fraction 21 contained prunolide F (**6**, 1.0 mg). Fraction 3 (A−D, 1.12 g) was purified on Sephadex LH-20 using MeOH as the eluent over 600 min. with fractions collected every 4 min. at a flow rate of 3 mL/min. Fractions 70-84 contained prunolide A (**1**, 17.3 mg) while fractions 135−141 contained pityriacitrin C (**11**, 0.7 mg). A sample of 100% MeOH and 20% H_2O/80% MeOH VLC fractions were extracted in DCM (1.12 g) and separated by preparative RP HPLC (Betasil C_{18} 5μm 100 Å, 21.2 mm x 150 mm) eluting from 100% H_2O to 100% MeOH 90 min. at a flow rate of 9 mL/min with fractions collected each min. Fractions 39−46 were recombined and further purified by preparative RP HPLC (Zorbax SB-Phenyl C_{18}, 21.2 mm x 150 mm) using an optimised solvent gradient from 25% H_2O/75% MeOH to 100% MeOH over 70 min. with the column left to elute at 100% MeOH for a further 10 min. (flow rate 9 mL/min, fractions collected each min.). Fraction 49 afforded prunolide H (**8**, 1.0 mg), while fractions 55-56 contained prunolide B (**2**, 2.2 mg).

Prunolide D (**4**): yellow amorphous solid; $[\alpha]_D^{23}$ +4.5 (*c* 0.05, MeOH); UV (MeOH) λ_{max} (log ε) 319 (6.3) nm; ^{1}H and ^{13}C NMR data, Table 1; HRESIMS *m/z* 653.0278 $[M - H]^-$ (calcd for $C_{34}H_{20}{}^{81}BrO_9^-$, 653.0270).

Prunolide E (**5**): yellow amorphous solid; $[\alpha]_D^{23}$ +4.8 (*c* 0.04, MeOH); UV (MeOH) λ_{max} (log ε) 318 (6.3) nm; ^{1}H and ^{13}C NMR data, Table 1; HRESIMS *m/z* 653.0274 $[M - H]^-$ (calcd for $C_{34}H_{20}{}^{81}BrO_9^-$, 653.0270).

Prunolide F (**6**): yellow amorphous solid; $[\alpha]_D^{23}$ +6.5. (*c* 0.02, MeOH); UV (MeOH) λ_{max} (log ε) 389 (3.9), 313 (4.1), 282 (4.0) nm; ^{1}H and ^{13}C NMR data, Table 1; HRESIMS *m/z* 810.8458 $[M - H]^-$ (calcd for $C_{34}H_{18}{}^{81}Br_2{}^{79}BrO_9{}^-$, 810.8459).

Prunolide G (**7**): yellow amorphous solid; $[\alpha]_D^{23}$ +5.7 (*c* 0.02, MeOH); UV (MeOH) λ_{max} (log ε) 390 (4.4), 289 (4.6) nm; ^{1}H and ^{13}C NMR data, Table 1; HRESIMS *m/z* 968.6646 $[M - H]^-$ (calcd for $C_{34}H_{16}{}^{81}Br_3{}^{79}Br_2O_9{}^-$, 968.6644).

Prunolide H (**8**): yellow amorphous solid; $[\alpha]_D^{23}$ +6.7 (*c* 0.02, MeOH); UV (MeOH) λ_{max} (log ε) 377 (4.1), 317 (4.2) nm;^{1}H and ^{13}C NMR data, Table 2; HRESIMS *m/z* 888.7596 $[M - H]^-$ (calcd for $C_{34}H_{17}{}^{81}Br_2{}^{79}Br_2O_9{}^-$, 888.7564).

Prunolide I (**9**): yellow amorphous solid; $[\alpha]_D^{23}$ +3.2 (*c* 0.02, MeOH); UV (MeOH) λ_{max} (log ε) 380 (4.5), 313 (3.7) nm; ^{1}H and ^{13}C NMR data, Table 2; HRESIMS *m/z* 730.9375 $[M - H]^-$ (calcd for $C_{34}H_{19}{}^{81}Br{}^{79}BrO_9{}^-$, 730.9375),

cis-Prunolide C (**10**): yellow amorphous solid; (*c* 0.04, MeOH); UV (MeOH) λ_{max} (log ε) 317 (6.8) nm; ^{1}H and ^{13}C NMR data, Table 2; HRESIMS *m/z* 573.1201 $[M - H]^-$ (calcd for $C_{34}H_{21}O_9{}^-$, 573.1185).

Pityriacitrin C (**11**): brown amorphous solid; UV (MeOH) λ_{max} (log ε) 388 (4.0), 366 (4.0), 267 (4.4), 257 (4.4) nm; ^{1}H and ^{13}C NMR data, Table 3; HRESIMS *m/z* 591.8634 $[M - H]^-$ (calcd for $C_{21}H_{10}{}^{81}Br{}^{79}BrN_3O_6S^-$, 591.8637).

***In vitro* α- Synuclein MS-Binding Assay**. α-Synuclein protein solutions (10 μM) were prepared in 10 mM ammonium acetate. Purified compounds (100 μM) were dissolved in 100% MeOH and incubated with α-syn at rt for 3 h. Protein-ligand interactions were analyzed using (+) HRESIMS calibrated with sodium trifluoroacetate (0.1 mg/mL) with the following parameters: nebulizer 2.0 Bar; dry gas 7 L/min; dry temp 150 °C; funnel I RF 400 Vpp; end plate offset 500 V; capillary 4500 V; ISCID 0.0 ev; ion energy 4.0 eV; transfer time 100 μs; multipole RF 800 Vpp; collision RF 1200 Vpp; prepulse storage 10 μs; spectra rate: 2×100 Hz. The resulting spectra were analyzed for additional peaks representing complexes formed between α-syn and active compounds.

***In vitro* α-Synuclein ThT Aggregation Assay**. Stock solutions (5mM) of Thioflavin T (ThT) were prepared in a glycine-NaOH buffer with a pH of 8.0. Homogenously monomeric α-syn was produced with the commonly used protocol presented by Rahimi et al to ensure consistent results.[31] The α-syn monomers (87.5 μM) were carefully dissolved in a saline tris buffer and filtered through 0.22 µm filters. The aggregation assay was performed in 96 well plates with each well containing a teflon polyball (1/8'' diameter), 80 µM α-syn, 50 µM thioflavin T, 80-400 µM test compounds and saline Tris buffer up to a final volume of 150 µL. Plates were shaken at 100 rpm and incubated at 37 °C for 36 h. Every 6 h the fluorescent intensity of each well was measured using a Tecan Spark Plate Reader by exciting at 460 nm and collecting the emission intensity at 500 nm. Each sample was measured in triplicate and each plate contained three negative controls (α-syn in the absence of compounds). The averaged ThT fluorescence of these wells was normalised to 100% aggregation. Each plate also contained three positive controls (α-syn in the presence of the common positive control epigallocatechin gallate to ensure reproducibility. The fluorescence intensity of the samples was compared to the negative controls to obtain the overall percentage inhibition.

Pre-formed Fibril (PFF) Induced α-Synuclein Aggregation in Primary Midbrain Cultures. Primary embryonic mouse midbrain cultures were isolated as described previously and plated in 96-well black optically clear bottom plates (6005182, PerkinElmer).[4] Recombinant wild-type mouse α-syn PFFs (SPR-324, StressMarq) were diluted in PBS (100 µg/mL) and sonicated in Bioruptor sonicator (Diagenode, Liege, Belgium) at high power with water bath temperature at 4 °C for 10 cycles, 30 s ON/30 s OFF. PFFs were added to culture media to final concentration of 2.5 µg/mL on day in vitro (DIV) 8; ~15 min. after the addition of PFFs, corresponding wells were treated with aforementioned concentrations of prunolides A, B, C (**1**-**3**), 50 ng/mL recombinant human GDNF protein (Icosagen, PeproTech) or 0.1% DMSO as vehicle (VEH) control. On DIV15 the cultures were fixed with 4% paraformaldehyde (PFA) for 20 min at rt and stored in PBS at 4 °C. Immunostaining was done as described elsewhere.[4,9] Briefly, fixed cells were twice rinsed with PBS, then permeabilized for 15 min with 0.2% Triton X-100 in PBS (PBST) and blocked for 1 h with 5% normal horse serum in PBST. The incubation with primary antibodies (ab1542, polyclonal sheep anti-TH, Millipore; ab51253, monoclonal rabbit anti-phosphoSer129-α-synuclein, Abcam; both at 1:2000 dilution) in 5% normal horse serum in PBST was done at 4 °C overnight. After thrice rinse with PBS, 1 h incubation with secondary antibodies (A11015, donkey anti-sheep AlexaFluor 488, Thermo Fisher; A31573, donkey anti-rabbit AlexaFluor 647, Thermo Fisher Scientific; both at 1:500 dilution), at rt, then PBS rinse was repeated, the cellular nuclei were stained for 10 min with 200 ng/mL 4',6-diamidino-2-phenylindole (DAPI). Plates were stored at 4 °C until imaging with ImageXpress Micro Automated Imaging System (Molecular Devices) fitted with 10× objective. From each well, nine view fields were acquired, covering entire midbrain culture. Quantification of TH-positive cells with or without Lewy body (LB)-like pSyn-positive aggregates was performed with CellProfiler 4.1.3 and CellAnalyst 2.2.1 software packages.[32] Detailed CellProfiler image analysis pipelines can be found elsewhere.[4]

Briefly, the numbers of TH neurons per well were quantified, then the classified TH neurons were grouped into pSyn-positive and pSyn-negative, utilizing supervised machine learning provided by aforementioned open-access software packages.[32] Summary of the experiment and example image for classification are shown in **Figure S66** of Supporting Information.

Data from at least three biological repeats (independent primary culture preparations with at least three wells per treatment condition on each plate) was analyzed with one-way or two-way randomized block ANOVA design, matching groups from different plates, followed by two-stage linear step-up procedure of Benjamini, Krieger and Yekutieli. [30,33] All statistical analyses were performed in GraphPad Prism 9 software. All data related to TH neurons were represented as means ± SD.

Antiplasmodial Image-Based Assay. Compounds **1**−**3** and **11** were evaluated for antiplasmodial activity using an imaging assay previously reported by Duffy and Avery.[34] In brief, compounds were tested at concentrations ranging from 0.4 *n*M−40 μM in a 16−point CRC format (N=2) against *Plasmodium falciparum* 3D7 parasites. Compounds were incubated in CellCarrier-384 well imaging plates in the presence of 2% parasitemia at 0.3% hematocrit in 50 μL total assay volume for 72 h at 37 °C, 5% O_2, 5% CO_2 and 90% N_2. Plates were then stained with DAPI and images acquired using an Opera confocal imaging system (Perkin Elmer). Analis was undertaken using Alcapella (PerkinElmer) software. Pyrimethamine, puromycin, and artesunate were included as assay controls. Normalized percent inhibition data was obtained using in-plate positive (5 μM puromycin) and negative (0.4% DMSO) controls; and utilised to calculate IC_{50} values. Data was graphed using nonlinear regression and sigmoidal dose-response using GraphPad Prism software version 6.

Cytotoxicity Assay. The cytotoxicity of **1**−**3** and **11** was determined using a human embryonic kidney cancer cell line (HEK293) as previously described by Fletcher and Avery.[35] Compounds were added to TC-treated 384-well Falcon plates containing 2000 HEK293 cells

per well and incubated for 72 h at 37 °C. Media was subsequently removed, replaced with 44 μM resazurin and plates incubated for 6 h. Fluorescence intensity was measured using an EnVision (PerkinElmer) plate reader. Cytotoxicty was determined by cell viability using 40 μM puromycin (positive) and 0.4% DMSO (negative) controls, and IC_{50} values calculated using GraphPad Prism software version 6.

Antibacterial Assay. The Gram-positive antibacterial activity of **1**−**7** and **10** was determined against wild-type methicillin-sensitive (ATCC 25923 MSSA) and methicillin-resistant (ATCC 43300 MRSA) *Staphylococcus aureus*. Stock solutions were prepared in DMSO at 2.0 μM for **1**−**3** and at 1.5 μM for **4**−**7** and **10**, from which stock plates were prepared by preforming a ten-fold, 1:2 serial dilution. Fusidic acid (IC_{50} <0.1 μM) was used as a positive control and 5% DMSO was used as a negative control. Overnight cultures were prepared by aseptically transferring a colony into 10 mL of sterile lysogeny broth and incubating for 16-18 h at 37.5 °C, from which the inoculate was prepared by adjusting the overnight culture to 5 × 10^5 CFU/mL. The assay was performed in sterile 96-well plates, and to each well 25 μL of double strength lysogeny broth, 5 μL of the stock solution, 20 μL of sterile H_2O and 50 μL of the inoculate was sequentially added. Plates were then incubated for 18 h at 37.5 °C while been shaken at 100 rpm. 10 μL of 704 μM resazurin (sodium salt, Sigma Aldrich) was then added to all wells and the assay plates incubated for a further 1 h. Resazurin reduction was recorded on a BMG LABTECH, FLUOstar Omega fluorescent plate reader (ex 544 nm, em 590 nm). All experiments were run in triplet over three consecutive days. IC_{50s} were calculated in GraphPad Prism (version 5) using the log(inhibitor) vs. response (Variable slope) equation.

ASSOCIATED CONTENT

Supporting Information.

Electronic supplementary information is available free of charge on the ACS Publications website at DOI:

1D and 2D NMR spectra for **4**−**11**, targeted MS/MS fragmentation spectrometric data for **11** and antiplasmodial, antibacterial and α-syn biological data for **1-11** (PDF).

AUTHOR INFORMATION

Notes

The authors assert no competing financial interests.

ACKNOWLEDGMENTS

This work was funded by an Australian Postgraduate Award (APA) provided by the Australian Commonwealth Government to DCH and DWP; the Academy of Finland grants #293392, #319195 to AD, and the University of Helsinki Doctoral Program on Drug Research funding to SE. We extend thanks to Dr W. Loa-Kum-Cheung, E. K. Kennedy, R. Stewart and A. Boyle for technical assistance. We thank J. Kennedy (Queensland Museum) for taxonomic identification of the ascidian. We gratefully acknowledge the Australian Red Cross for the provision of blood essential for antiplasmodial testing.

References

(1) Pujols, J.; Peña-Díaz, S.; Conde-Giménez, M.; Pinheiro, F.; Navarro, S.; Sancho, J.; Ventura, S. *Int. J. Mol. Sci.* **2017**, *18*, 478.

(2) Young, L. M.; Saunders, J. C.; Mahood, R. A.; Revill, C. H.; Foster, R. J.; Tu, L. H.; Raleigh, D. P.; Radford, S. E.; Ashcroft, A. E. *Nat. Chem.* **2015**, *7*, 73–81.

(3) Houlden, H.; Singleton, A. B. *Acta. Neuropathol.* **2012**, *124*, 325–338.

(4) Er, S.; Hlushchuk, I.; Airavaara, M.; Chmielarz, P.; Domanskyi, A. *J. Vis. Exp.* **2020**, *162*, 1-20.

(5) Anderson, J.P.; Walker, D.E.; Goldstein, J.M.; de Laat, R.; Banducci, K.; Caccavello, R.J.; Barbour, R.; Huang, J.; Kling, K.; Lee, M.; Diep, L.; Keim, P.S.; Shen, X.; Chataway, T.; Schlossmacher, M.G.; Seubert, P.; Schenk, D.; Sinha, S.; Gai, W.P.; Chilcote, T.J. *J. Biol. Chem.* **2006**, *281*, 29739-52.

(6) Velander, P.; Wu, L.; Henderson, F.; Zhang, S.; Bevan, D. R.; Xu, B. *Pharmacol.* **2017**, *139*, 40–55.

(7) Volpicelli-Daley, L.A.; Luk, K.C.; Patel, T.P.; Tanik, S.A.; Riddle, D.M.; Stieber, A.; Meaney, D.F.; Trojanowski, J.Q.; Lee, V.M. *Neuron*. **2011**, *72*, 57-71.

(8) Volpicelli-Daley, L.A.; Luk, K.C.; Lee, V.M. *Nat Protoc*. **2014**, *9*, 2135-2146.

(9) Chmielarz, P.; Er, S.; Konovalova, J.; Bandres, L.; Hlushchuk, I.; Albert, K.; Panhelainen, A.; Luk, K.; Airavaara, M.; Domanskyi, A. *Mov Disord*. **2020**, *35*, 2279-2289.

(10) Hlushchuk, I.; Ruskoaho, H.; Domanskyi, A.; Airavaara, M.; Välimäki, M. *ACS Chem. Neurosci.* **2021**, *12*, 2273-2279.

(11) Blunt, J. W.; Carroll, A. R.; Copp, B. R.; Davis, R. A.; Keyzers, R. A.; Prinsep, M. R. *Nat. Prod. Rep.* **2018**, *35*, 8–53.

(12) Marine Pharmacology https://www.marinepharmacology.org/approved (accessed May 20, 2021).

(13) White, K. M.; Rosales, R.; Yildiz, S.; Kehrer, T.; Miorin, L.; Moreno, E.; Jangra, S.; Uccellini, M. B.; Rathnasinghe, R.; Coughlan, L.; Martinez-Romero, C.; Batra, J.; Rojc, A.; Bouhaddou, M.; Fabius, J. M.; Obernier, K.; Dejosez, M.; Guillén, M. J.; Losada, A.; Avilés, P.; Schotsaert, M.; Zwaka, T.; Vignuzzi, M.; Shokat, K. M.; Krogan, N. J.; García-Sastre, A. *Science* **2021**, *371*, 926–931.

(14) Bracegirdle, J.; Keyzers, R. A. *Curr. Pharm. Des.* **2020**, 26, 4351–4360.

(15) Bracegirdle, J.; Stevenson, L. J.; Sharrock, A. V.; Page, M. J.; Vorster, J. A.; Owen, J. G.; Ackerley, D. F.; Keyzers, R. A. *J. Nat. Prod.* **2021**, *84*, 544–547.

(16) Bracegirdle, J.; Stevenson, L. J.; Page, M. J.; Owen, J. G.; Keyzers, R. A. *Mar. Drugs* **2020**, *18*, 337.

(17) Ortega, M. J.; Zubía, E.; Ocaña, J. M.; Naranjo, S.; Salvá, J. *Tetrahedron* **2000**, *56*, 3963–3967.

(18) Sikorska, J.; Parker-Nance, S.; Davies-Coleman, M. T.; Vining, O. B.; Sikora, A. E.; McPhail, K. L. *J. Nat. Prod.* **2012**, *75*, 1824–1827.

(19) Smitha, D.; Kumar, M. M. K.; Ramana, H.; Rao, D. V. *Nat. Prod. Res.* **2014**, *28*, 12-17.

(20) Smith, C. J.; Hettich, R. L.; Jompa, J.; Tahir, A.; Buchanan, M. V; Ireland, C. M. *J. Org. Chem.* **1998**, *63*, 4147–4150.

(21) Wang, W.; Kim, H.; Patil, R. S.; Giri, A. G.; Won, D. H.; Hahn, D.; Sung, Y.; Lee, J.; Choi, H.; Nam, S. J.; et al. Cadiolides J–M. *Bioorg. Med. Chem. Lett.* **2017**, *27*, 574–577.

(22) Jennings, L. K.; Robertson, L. P.; Rudolph, K. E.; Munn, A. L.; Carroll, A. R. *J. Nat. Prod.* **2019**, *82*, 2620–2626.

(23) Carroll, A. R.; Healy, P. C.; Quinn, R. J.; Tranter, C. J. *J. Org. Chem.* **1999**, *64*, 2680–2682.

(24) Sofikiti, N.; Tofi, M.; Montagnon, T.; Vassilikogiannakis, G.; Stratakis, M. *Org. Lett.* **2005**, *7*, 2357–2359.

(25) Holland, D. C.; Kiefel, M. J.; Carroll, A. R. *J. Org. Chem.* **2020**, *85*, 3490–3496.

(26) Meragelman, K. M.; West, L. M.; Northcote, P. T.; Pannell, L. K.; McKee, T. C.; Boyd, M. R. *J. Org. Chem.* **2002**, *67*, 6671–6677.

(27) Irlinger, B.; Bartsch, A.; Krämer, H. J.; Mayser, P.; Steglich, W. *Helv. Chim. Acta* **2005**, *88*, 1472–1485.

(28) Mayser, P.; Schäfer, U.; Krämer, H. J.; Irlinger, B.; Steglich, W. *Arch. Dermatol. Res.* **2002**, *294*, 131–134.

(29) MarinLit http://pubs.rsc.org/marinlit/ (accessed Jul 31, 2021).

(30) Benjamini, Y.; Krieger, A. M.; Yekutieli, D. *Biometrika* **2006**, *93*, 491–507.

(31) Rahimi, F.; Maiti, P.; Bitan, G. *J. Vis. Exp.* **2009**, *23*, 1071-1073.

(32) McQuin, C.; Goodman, A.; Chernyshev, V.; Kamentsky, L.; Cimini, B.A.; Karhohs, K.W.; Doan, M.; Ding, L.; Rafelski, S.M.; Thirstrup, D.; Wiegraebe, W.; Singh, S.; Becker, T.; Caicedo, J.C.; Carpenter, A.E. *PLoS Biol*. **2018**, *16*, 1-17.

(33) Lew, M. *Br. J. Pharmacol.* **2007**, *152*, 295-298.

(34) Duffy, S.; Avery, V. M. *Am. J. Trop. Med. Hyg.* **2012**, *86*, 84–92.

(35) Fletcher, S.; Avery, V. M. *Malar. J.* **2014**, *13*, 1–17.

TOC